Ab initio electronic transport and thermoelectric properties of solids from full and range-separated hybrid functionals

This manuscript was accepted by J. Chem. Phys. Click here to see the version of record.

Ab initio electronic transport and thermoelectric properties of solids from full and range-separated hybrid functionals.

Giuseppe Sansone,[1] Andrea Ferretti,[2] and Lorenzo Maschio[3]

[1]*Dipartimento di Chimica, Università di Torino, Via P. Giuria 5, 10125 Torino, Italy*

[2]*S3 Center, Istituto Nanoscienze, CNR, Via Campi 213/A, 41125, Modena, Italy*

[3]*Dipartimento di Chimica, C3S centre, NIS centre, Università di Torino, Via P. Giuria 5, 10125 Torino, Italy**

(Dated: August 21, 2017)

Abstract

Within the semiclassical Boltzmann transport theory in the constant relaxation-time approximation, we perform an *ab initio* study of the transport properties of selected systems, including crystalline solids and nanostructures. A local (Gaussian) basis set is adopted and exploited to analytically evaluate band velocities as well as to access full and range-separated hybrid functionals (such as B3LYP, PBE0 or HSE06) at a moderate computational cost. As a consequence of the analytical derivative, our approach is computationally efficient and does not suffer from problems related to bands crossings.

We investigate and compare the performance of a variety of hybrid functionals in evaluating Boltzmann conductivity. Demonstrative examples include silicon and aluminum bulk crystals as well as two thermoelectric materials ($CoSb_3$, Bi_2Te_3). We observe that hybrid functionals, other than providing more realistic band gaps – as expected – lead to larger band widths and hence allow for a better estimate of transport properties, also in metallic systems. As a nanostructure prototype we also investigate conductivity in Boron-Nitride substituted graphene, in which nanoribbons (nanoroads) alternate with BN ones.

This manuscript was accepted by J. Chem. Phys. Click here to see the version of record.

I. INTRODUCTION

Properties of solids that are related to the motion of electrons through the material, such as conductivity or thermoelectricity, evidently are of primary interest for the technological development. As a direct consequence, the ability to accurately simulate such properties can be key to foster the development of new materials and devices, as well as to understand their fundamental physics underpinning the relevant features.

Electrical and thermal conductivities are always taken into account in the design of any electronic device, either as desired or undesired properties. As an example, great interest resides in the possibility to have materials with strongly anisotropic conductivities. Similarly, thermoelectric materials are one among the "hot" topics of today's science, under the promise of converting waste heat into useful electricity.[1] The most important quantity to look at, when trying to assess the potential interest of a thermoelectric material, is the dimensionless figure-of-merit, ZT,

$$ZT = \frac{\sigma S^2 T}{\kappa} \tag{1}$$

where T is the temperature, S is the Seebeck coefficient (measuring the average entropy carried by a charge in the material), σ is the electrical conductivity, and $\kappa = \kappa_p + \kappa_e$ is the thermal conductivity which is composed of phonon thermal conductivity, κ_p, and electronic thermal conductivity, κ_e. A large power factor (σS^2) means efficiency in the heat-electricity conversion, while a small thermal conductivity is required to maintain a temperature gradient and reduce conduction heat losses.[2,3]

As mentioned above, for the purpose of *in silico* characterization of crystalline solids there is much interest in obtaining an estimate of conductivity and thermoelectric power of materials. *ab initio* or *first principles* methods, such as provided by Kohn-Sham Density Functional Theory (DFT), are widely accepted as the best compromise between cost and accuracy. So far, to our knowledge, there exist two main codes that can post-process a DFT wavefunction for evaluating the electron transport properties through the solution of the Boltzmann transport equation: BoltzTrap[4] and BoltzWann.[5] From the theoretical point of view, the critical quantity that has to be calculated is the band velocity, that in atomic unit (a.u.) is expressed as the derivative of the band energies $E(i, \mathbf{k})$, with respect to a reciprocal space vector k_q

$$v_{i,q}(\mathbf{k}) = \frac{\partial E_i(\mathbf{k})}{\partial k_q} \quad . \tag{2}$$

The two abovementioned codes use different approaches for evaluation of such derivative. BoltzTrap relies on a Fourier expansion of the band energies and differentiates numerically. BoltzWann exploits a maximally-localized Wannier function basis, and after localization the band derivatives is evaluated analytically at each **k** point. Both approaches are now well assessed, but are eventually prone to suffer of stability issues due to the numerical accuracy of the procedure, entanglement of electronic bands, or rapidly increasing computational cost with system size and/or tightening of computational parameters.

In this work we exploit the local atom–centered Gaussian basis set implemented in the CRYSTAL code[6] to combine together the possibility to perform analytical derivatives of the electronic bands (to evaluate Boltzmann conductivity) with the numerical efficiency in treating non-local exchange and hybrid functionals. This allows us to investigate the performance of a variety of hybrid functionals in describing the electronic conductivity within the semiclassical Boltzmann theory.

The paper is structured as follows. After some preliminaries on semiclassical Boltzmann transport theory in Sec. II. The working equations are derived and details of implementation are discussed in Section III. The developed algorithm are then, in Section IV, applied to the study of prototypical systems, as bulk silicon and aluminum as well as two thermoelectric materials ($CoSb_3$, Bi_2Te_3). As a possible real-life application, we finally investigate conductivity in Boron-Nitride substituted Graphene (BNsG).

II. SEMICLASSICAL BOLTZMANN TRANSPORT THEORY

A detailed description of the semiclassical Boltzmann transport theory is beyond the scope of this article. However, since it is central to the present discussion, we briefly review its main results here. The reader is redirected to more specialized textbooks for more details.[7–9]

The thermoelectric processes linking non-equilibrium coupled processes such as the electrical and heat fluxes[10] were studied by Onsager and Callen[11–13] in the first half of the XX$^{\text{th}}$ century, in the framework of the thermodynamics of dissipative system. In their model,

This manuscript was accepted by J. Chem. Phys. Click here to see the version of record.

current densities can be expressed as

$$\underbrace{\begin{bmatrix}\mathbf{J}_E\\ \mathbf{J}_Q\end{bmatrix}}_{\text{current densities}} = \underbrace{\begin{bmatrix}\sigma & \sigma\mathbf{S}\\ \mathbf{T}\sigma\mathbf{S} & \kappa_{\text{el}}\end{bmatrix}}_{\text{transport coefficients}} \underbrace{\begin{bmatrix}-\nabla V\\ -\nabla T\end{bmatrix}}_{\text{forces}} \tag{3}$$

where $\mathbf{J}_E$ is the electrical current density, $\mathbf{J}_Q$ is the heat current density, σ is the electrical conductivity, $\mathbf{S}$ is the Seebeck coefficient, T the temperature, V the electric potential and κ_{el} the electron contribution to the thermal conductivity. Eq. (3) can be derived from Boltzmann's semiclassical transport theory,[14] providing the expressions of the three so-called transport coefficients: σ, $\sigma\mathbf{S}$ and κ_{el},

$$[\sigma]_{qr}(\mu,T) = e^2 \int \mathrm{d}E \Big(-\frac{\partial f_0}{\partial E}\Big)\Xi_{qr}(E) \tag{4}$$

$$[\sigma\mathbf{S}]_{qr}(\mu,T) = \frac{e}{T} \int \mathrm{d}E \Big(-\frac{\partial f_0}{\partial E}\Big)(E-\mu)\Xi_{qr}(E) \tag{5}$$

$$[\kappa_{el}]_{qr}(\mu,T) = \frac{1}{T} \int \mathrm{d}E \Big(-\frac{\partial f_0}{\partial E}\Big)(E-\mu)^2\Xi_{qr}(E) \tag{6}$$

where μ is the chemical potential or the Fermi level, E is the energy, f_0 is the Fermi-Dirac distribution and Ξ is the transport distribution function (TDF). In the above equations, the core of the transport coefficients, Ξ, is defined as[15,16]

$$\Xi_{qr}(E) = \tau \sum_{\mathbf{k}} \frac{1}{N_{\mathbf{k}}} \frac{1}{V} \sum_{i,j} v_{i,q}(\mathbf{k}) v_{j,r}(\mathbf{k}) \delta\big(E - E_i(\mathbf{k})\big) \tag{7}$$

where $v_{i,q}(\mathbf{k})$ is the velocity of the i-th band calculated along the direction q, τ is the lifetime which we assumed to be not dependent on $\mathbf{k}$ according to the constant relax time approximation.

III. THEORY AND IMPLEMENTATION

A. Theoretical Framework

We solve the Hartree-Fock or Kohn-Sham equations in the LCAO (Linear Combination of Atomic Orbitals) approach.[17] In LCAO each Crystalline Orbital (CO), $\psi_i(\mathbf{r};\mathbf{k})$, is expressed

a linear combination of Bloch functions (BFs), $\phi_\mu(\mathbf{r};\mathbf{k})$. These, in turn, are formally defined in terms of local functions, $\varphi_\mu(\mathbf{r})$, referred to as Atomic Orbitals (AOs):

$$\psi_i(\mathbf{r};\mathbf{k}) = \sum_\mu c_{\mu,i}(\mathbf{k})\phi_\mu(\mathbf{r};\mathbf{k}) \tag{8}$$

$$\phi_\mu(\mathbf{r};\mathbf{k}) = \sum_{\mathbf{g}} \varphi_\mu(\mathbf{r}-\mathbf{A}_\mu-\mathbf{g})\; e^{i\mathbf{k}\cdot\mathbf{g}} \tag{9}$$

where $\mathbf{r}$ is a cartesian vector and $\mathbf{g}$ is a lattice vector, both in direct space. $\varphi_\mu(\mathbf{r}-\mathbf{A}_\mu-\mathbf{g})$ is one – or a contraction of several – Gaussian(s) function centered on an atom having cartesian coordinates $\mathbf{A}_\mu$. The $\mathbf{g}$ summation is in principle infinite. However, Eq. (9) is never used explicitly, and all lattice summations appearing in the working equations (see below) are screened according to suitable thresholds.

The matrix $\mathbf{C}(\mathbf{k})$ of the expansion coefficients of the Bloch functions, $c_{\mu,i}(\mathbf{k})$ appearing in Eq. (8), are calculated by solving the matrix equation for each reciprocal lattice vector, $\mathbf{k}$:

$$\mathbf{F}(\mathbf{k})\mathbf{C}(\mathbf{k}) = \mathbf{S}(\mathbf{k})\mathbf{C}(\mathbf{k})\mathbf{E}(\mathbf{k}) \tag{10}$$

where the coefficients are subject to the orthonormality condition

$$\mathbf{C}^\dagger(\mathbf{k})\mathbf{S}(\mathbf{k})\mathbf{C}(\mathbf{k}) = \mathbf{1} \tag{11}$$

Here $\mathbf{S}(\mathbf{k})$ is the reciprocal space image of the overlap matrix between basis functions,

$$\mathbf{S}(\mathbf{k}) = \sum_{\mathbf{g}} \mathbf{S}(\mathbf{g})\; e^{i\mathbf{k}\cdot\mathbf{g}} \quad , \tag{12}$$

and $\mathbf{F}(\mathbf{k})$ is the Fock matrix in reciprocal space:

$$\mathbf{F}(\mathbf{k}) = \sum_{\mathbf{g}} \mathbf{F}(\mathbf{g})\; e^{i\mathbf{k}\cdot\mathbf{g}} \quad . \tag{13}$$

By iteratively solving (10) we obtain the $\mathbf{E}(\mathbf{k})$ is the diagonal matrix of eigenvalues,

$$\mathbf{E}(\mathbf{k}) = \mathbf{C}^\dagger(\mathbf{k})\mathbf{F}(\mathbf{k})\mathbf{C}(\mathbf{k}) \tag{14}$$

yielding the energy bands. F is the usual Hartree-Fock (or Kohn-Sham) Hamiltonian, taking into account Ewald summations and spheropole terms for handling the otherwise non-convergent infinite Coulomb series – see for instance Eq. (5) of Ref. [18] or Eq. (11) of Ref. [19]; the reader can refer to Ref. [17] for a full discussion on the topic.

This manuscript was accepted by J. Chem. Phys. Click here to see the version of record.

B. Calculation of band velocities

The focus of the present development is in obtaining the band velocities, appearing in Eq. (7), as derivatives of the electronic bands, as in Eq. (2). By differentiating Eq. (10) with respect to a reciprocal space vector $\mathbf{k}$, we obtain:

$$\begin{aligned}\frac{\partial \mathbf{F}(\mathbf{k})}{\partial \mathbf{k}}\mathbf{C}(\mathbf{k})+\mathbf{F}(\mathbf{k})\frac{\partial \mathbf{C}(\mathbf{k})}{\partial \mathbf{k}} = \frac{\partial \mathbf{S}(\mathbf{k})}{\partial \mathbf{k}}\mathbf{C}(\mathbf{k})\mathbf{E}(\mathbf{k})+ \\ + \mathbf{S}(\mathbf{k})\frac{\partial \mathbf{C}(\mathbf{k})}{\partial \mathbf{k}}\mathbf{E}(\mathbf{k}) + \mathbf{S}(\mathbf{k})\mathbf{C}(\mathbf{k})\frac{\partial \mathbf{E}(\mathbf{k})}{\partial \mathbf{k}}\end{aligned} \tag{15}$$

According to Refs. 20, 21 and 22, we express the derivative of the coefficients with respect to the quasi-momentum index $\mathbf{k}$ as:

$$\frac{\partial \mathbf{C}(\mathbf{k})}{\partial \mathbf{k}} = \mathbf{C}(\mathbf{k})\mathbf{Q}(\mathbf{k}) \tag{16}$$

The explicit form of the $\mathbf{Q}(\mathbf{k})$ matrix can be found in Ref. [23]. However, as we will show shortly, it will not be needed here.

By multiplying Eq. (15) on the left by $\mathbf{C}(\mathbf{k})^\dagger$, and exploiting Eqs. (11), (14) and (16), we obtain:

$$\begin{aligned}\mathbf{C}^\dagger(\mathbf{k})\frac{\partial \mathbf{F}(\mathbf{k})}{\partial \mathbf{k}}\mathbf{C}(\mathbf{k}) + \mathbf{E}(\mathbf{k})\mathbf{Q}(\mathbf{k}) = \\ \mathbf{C}^\dagger(\mathbf{k})\frac{\partial \mathbf{S}(\mathbf{k})}{\partial \mathbf{k}}\mathbf{C}(\mathbf{k})\mathbf{E}(\mathbf{k}) + \mathbf{Q}(\mathbf{k})\mathbf{E}(\mathbf{k}) + \frac{\partial \mathbf{E}(\mathbf{k})}{\partial \mathbf{k}}\end{aligned} \tag{17}$$

If we are interested only in the diagonal terms of $\frac{\partial \mathbf{E}(\mathbf{k})}{\partial \mathbf{k}}$, we can exploit the fact that $E_i(\mathbf{k})\mathbf{Q}(\mathbf{k}) = \mathbf{Q}(\mathbf{k})E_i(\mathbf{k})$, and then write:

$$\begin{aligned}\frac{\partial E_i(\mathbf{k})}{\partial \mathbf{k}} = \left[\mathbf{C}^\dagger(\mathbf{k})\frac{\partial \mathbf{F}(\mathbf{k})}{\partial \mathbf{k}}\mathbf{C}(\mathbf{k})\right]_{ii} \\ - \left[\mathbf{C}^\dagger(\mathbf{k})\frac{\partial \mathbf{S}(\mathbf{k})}{\partial \mathbf{k}}\mathbf{C}(\mathbf{k})\mathbf{E}(\mathbf{k})\right]_{ii} = v_{i,q}(\mathbf{k})\end{aligned} \tag{18}$$

that is the desired result where, as anticipated, the $\mathbf{Q}(\mathbf{k})$ matrix does not appear anymore, and hence we have all the required ingredients just from solving the self-consistent field equations (10). We note that the same result, in a different context, was obtained by Champagne *et al.*[20] and Otto *et al.*[21]

In a local basis set it is trivial to obtain the $\mathbf{k}-$vector derivative of the Fock and overlap matrices required by Eq. (18). After (13) :

$$\frac{\partial \mathbf{F}(\mathbf{k})}{\partial k_q} = \sum_{\mathbf{g}} i\, g_q\, \mathbf{F}(\mathbf{g})\, e^{i\mathbf{k}\cdot\mathbf{g}} \tag{19}$$

and similarly

$$\frac{\partial \mathbf{S}(\mathbf{k})}{\partial k_q} = \sum_{\mathbf{g}} i\, g_q\, \mathbf{S}(\mathbf{g})\; e^{i\mathbf{k}\cdot\mathbf{g}} \tag{20}$$

where q is a cartesian direction.

A similar technique as the one outlined in this section has been used in Ref.24 to compute the real and complex band structures of one dimensional systems.

IV. RESULTS

In this section we present our electron transport calculation on several prototypical solids, with a focus on the role of the main choices of computational setting, namely the basis set and Hamiltonian. As we will show, the use of hybrid functionals does make a difference, specially for semiconductors.

Using Eq. (7), even if within the constant relaxation time approximation, requires the knowledge of the lifetime τ. Since the *ab initio* evaluation of such quantity is not yet available in our approach, we rely here on experimentally determined values, when available. The values we have adopted are τ_{xx}=22fs and τ_{zz}=21fs for Bi_2Te_3, τ=10fs for $CoSb_3$ and Silicon, τ=8fs for Al. See Supplementary Information for more details.

All results have been obtained with a pre-release version of the CRYSTAL17 program[25] featuring the newly implemented DIIS convergence accelerator for periodic systems.[26]

A. Conductivity

We have computed the electrical conductivity – according to Eq. (4) – for two prototypical systems: solid Aluminum (fcc lattice), as a representative of a metallic system, and Silicon, the most representative and well-studied semiconductor.

For each system we have benchmarked the performance of different Hamiltonians (functionals) and basis sets. We can list the several functionals tested, grouped into different categories according to the level of approximation and the amount of Hartree-Fock (HF) exchange included:

- Local Density Approximation (LDA).[27,28]

This manuscript was accepted by J. Chem. Phys. Click here to see the version of record.

- Gradient-Generalized functionals: PW91[29], PBE[30], WCPBE[31,32]
- Global hybrid functionals containing different percentage of HF exchange: B3LYP,[33,34] PBE0,[35] PW1PW.[36]
- Range–separated hybrid functionals either with short-range or long-range HF exchange: M06,[37] HSE06,[30,38] LC-ω-BLYP.[39]
- Pure Hartree-Fock

Similarly we have adopted basis sets of different quality, either adopting pseudopotentials for core shells or all-electron ones, whose details can be found in the Supplementary Information.

In Table I we report, for the Aluminum bulk crystal, the value of the electrical conductivity at the Fermi level. It can be seen that, taking as a reference an experimental value of $36.5 \times 10^6 (\Omega \cdot \mathrm{m})^{-1}$,[40] pure functionals such as LDA or PBE systematically underestimate conductivity, with significant variations according to the basis set, while hybrid functionals yield consistently higher Fermi-level conductivities, even though the scattering of values for different basis sets is larger. Hamiltonians with long-range exchange, such as LCω-BLYP and HF, tend to overestimate conductivity and have convergence problems with more diffuse basis sets. Here, the overestimation effect comes from the increase in the band width due to the non-local exchange contribution.

In Figure 1 we report analogous results for bulk Silicon. Here it is seen that the shape of the conductivity profile is nearly independent on the functional, and mostly on basis sets as well (only 831G* and TZVP show a marked difference with respect to others). What makes a difference, here, is the ability of functionals to correctly reproduce the band gap of the system. The experimental indirect band gap is 1.17eV[41] which is correctly reproduced by hybrid functionals, and particularly HSE06 (see Table II). One might take into account an expected 0.1eV lowering correction due to spin-orbit coupling.[42]

B. Thermoelectric materials

In order to further validate the correctness and applicability of the approach presented in this paper, in Figs. 2 and 3 we present our results for the transport coefficients – Eqs. (4), (5)

and (6) – for two well-known thermoelectric materials, namely Bi_2Te_3 and $CoSb_3$. Details on the adopted basis set, computational parameters and structure can be found in the SI – however, in analogy with the case of Silicon, results are only mildly dependent on the basis set quality, and mainly to the extent it affects the band gap. Results are reported for three temperatures, 300, 500, and 700 K. In the left panel of both figures, the results obtained with a PBE functional[30] are reported, and can be compared with those in Figure 1 and 3 of Ref. [4] and in Figure 4 of Ref. [5]. The evident similarity of our results with previous approach, despite the difference in the underlying method for obtaining the wavefunctions (plane wave basis in those cases), is in our opinion a strong validation of the reliability of the treatment presented in this work. In the right panel of both Figs. 2 and 3 we report the same results obtained using the PBE0[35] hybrid functional.

It has to be underlined that the calculations presented here do not include spin-orbit coupling (SOC). In fact, for such topological insulators SOC has a significant effect in the correct description of the band gap. As shown by Crowley *et al.*[42,43] SOC lowers the band gap of Bi_2Te_3 by about 0.6eV. As a consequence, the band gaps for our calculation are expectedly larger than the experimental estimates ($\approx$0.15eV for Bi_2Te_3,[44] 0.118eV[45] – 0.22eV[16] for $CoSb_3$). Crowley *et al.*[42,43] have also widely discussed how non-hybrid functionals, like PBE, even if apparently closer to the experimental band gap, contain some wrong physics, while the band structure obtained by hybrid functionals well compare to the higher-level (and more expensive) G_0W_0 calculations.[46]

C. Graphene/h-BN nanoroads

As a demonstrative application of the new *ab initio* treatment of conductivity outlined in this paper, we have tackled the study of 2D heterostructures of Boron-Nitride substituted Graphene (BNsG), where the substitution pattern is such that nano-stripes of BN and C alternate in the plane. The structures we have studied are reported in the bottom panel of Figure 4 and have been picked among the many that have been studied by one of the authors in a previous work, focused on the peculiar features of their Raman spectrum.[47] The computational setup (basis set, thresholds, geometry) adopted here are exactly the same as used in that work.

In the top panel of Figure 4 the computed conductivity is plotted for pure graphene,

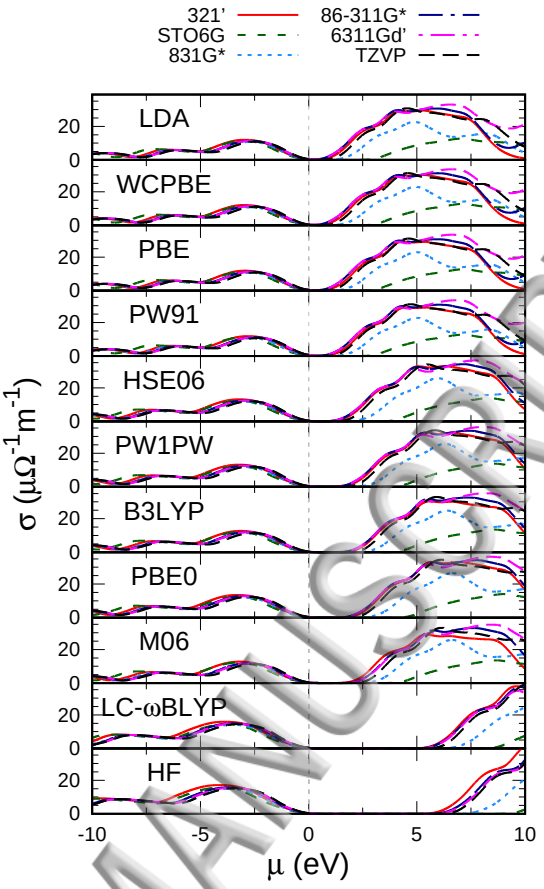

Figure 1: Electrical conductivity of bulk Silicon, evaluated for different functionals (panels) and basis sets (different lines).

and for two heterostructures. The in-plane conductivities in the direction parallel (σ_{xx}) and perpendicular (σ_{yy}) to the ribbon are reported for the latter. The well-known behaviour of graphene in the vicinity of the Fermi level is correctly reproduced by our calculations. As for the heterostructures, interestingly we see that little above the bottom of the conduction band, and little below the top of valence band, the nanoribbon shows a conductivity along the x direction that is comparable to that of graphene. The point of maximum conductivity is different in the two structures considered (0.8 / 1.2 eV) but the behaviour is similar. On the contrary, along the y direction the barrier of insulating BN stripes significantly reduces the conductivity, even more so for the thicker one, as expected. All the computational details can be found in Supplementary Information.

Table I: Conductivity of bulk Aluminum at the Fermi level for different functionals and basis sets. Values in $10^6(\Omega\cdot\mathrm{m})^{-1}$, to be compared with the experimental estimate of $36.5 \times 10^6(\Omega\cdot\mathrm{m})^{-1}$.[40]

DFT Functional	Basis Sets				
	321' [a)]	86-21G*	6311Gd'[a)]	TZVP	ECP-21G*
HF	/	44.26	/	38.55	40.87
LDA	26.99	25.15	25.75	20.06	24.94
PBE	25.99	24.36	25.22	20.16	24.97
PW91	26.16	24.60	25.36	20.12	24.93
WCPBE	26.01	24.48	25.31	20.15	24.96
B3LYP	31.95	29.05	29.44	23.84	28.75
PW1PW	30.47	27.73	28.55	23.99	29.42
PBE0	31.30	28.24	29.35	25.01	29.63
M06	30.24	27.85	29.17	24.88	28.97
HSE06	28.33	26.12	27.47	22.48	27.17
LC-ωBLYP	/	41.93	/	36.28	39.58

a) The most diffuse exponent have been rescaled, see SI for more details.

V. CONCLUSIONS

In this work we have described a novel implementation for calculating band velocities as the analytical derivative of electronic bands. This was made possible by the adoption of a basis set of local atom-centered orbitals (Gaussian functions) as adopted by the CRYSTAL code. Posed in the framework of semi-classical Boltzmann transport theory, this allowed us to devise a scheme for the calculation of electronic transport and thermoelectric properties of solids, that is both robust and simple to use – as it requires no input parameters from the user other than the reciprocal space sampling mesh (and, eventually, a smearing factor for the distribution function). Rooted in the use of a localized basis set, this approach can naturally be combined with the efficient use of hybrid functionals.

We have validated the correctness and the reliability of the approach on two well-known thermoelectric materials, $CoSb_3$ and Bi_2Te_3, and compared results with those available in the

Table II: Indirect silicon band gap calculated with different functionals using the 6311Gd' basis set.

Functional	Band Gap (eV)
LDA	0.53
WCPBE	0.53
PBE	0.63
PW91	0.64
HSE06	1.18
PW1PW	1.56
B3LYP	1.78
PBE0	1.77
M06	2.08
LC-ωBLYP	5.52
HF	6.22

literature. In addition, we have documented the effect of basis set and functional choice, with a focus on the hybrid functionals, on the evaluation of conductivity of a metallic (Aluminum) and a semiconducting (Silicon) system. Finally, directional electron conductivities of pure graphene and two boron nitride/graphene 2D structures were successfully computed.

Our results show that hybrid functionals tend systematically increase the Boltzmann conductivity with respect to local or semilocal functionals, such as LDA or GGA's. Contrary to the expected increased localization of the orbitals, the conductivity increase is connected to the larger band widths obtained with hybrid functionals.

Supplementary Material

See supplementary material for full details on crystal structures and computational setup.

* Electronic address: lorenzo.maschio@unito.it

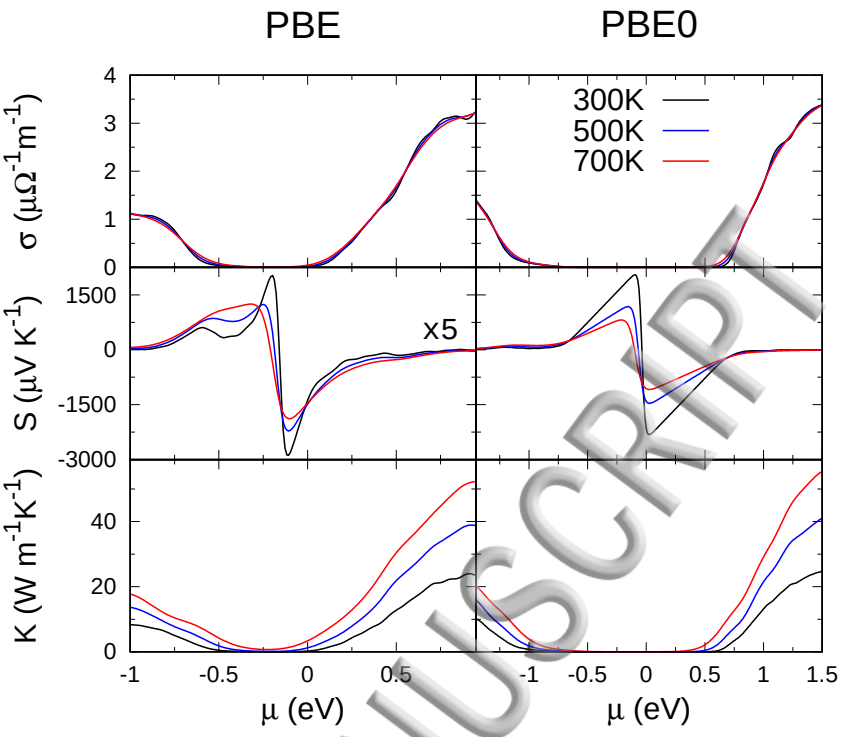

Figure 2: $CoSb_3$: electron conductivity (top panel), Seebeck (middle panel) and electronic thermal conductivity (bottom panel) as obtained for different temperatures and two different functionals: one pure GGA (PBE) and one hybrid (PBE0). The Seebeck curve for the PBE functional has been magnified by a factor of 5 in order to bring it to the same scale as the PBE0 one.

[1] J. P. Heremans, M. S. Dresselhaus, L. E. Bell, and D. T. Morelli, Nat. Nanotech. **8**, 471 (2013).

[2] Z. Tian, S. Lee, and G. Chen, Ann. Rev. Heat Transfer **17**, 425 (2014).

[3] J. R. Sootsman, D. Y. Chung, and M. G. Kanatzidis, Angew. Chem. Int. Ed. **48**, 8616 (2009).

[4] G. K. H. Madsen and D. J. Singh, Comput. Phys. Comm. **175**, 67 (2006).

[5] G. Pizzi, D. Volja, B. Kozinsky, M. Fornari, and N. Marzari, Comput. Phys. Comm. **185**, 422 (2014).

[6] R. Dovesi et al., Int. J. Quantum Chem. **114**, 1287 (2014).

[7] N. Ashcroft and N. Mermin, *Solid state physics* (Saunders College, Philadelphia, 1976).

[8] J. Ziman, *Principles of the Theory of Solids* (Cambridge University Press, London, England, 1964).

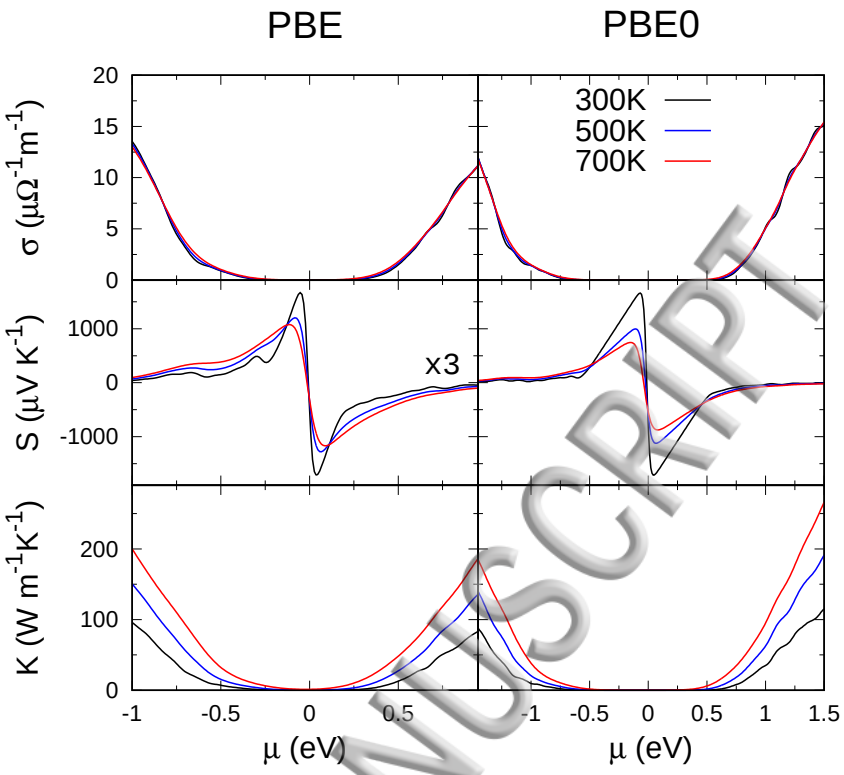

Figure 3: Bi_2Te_3: electron conductivity (top panel), Seebeck (middle panel) and electronic thermal conductivity (bottom panel) as obtained for different temperatures and two different functionals: one pure GGA (PBE) and one hybrid (PBE0). The Seebeck curve for the PBE functional has been magnified by a factor of 3 in order to bring it to the same scale as the PBE0 one.

[9] G. Grosso and G. P. Parravicini, *Solid State Physics* (Academic Press, 2000).

[10] C. Goupil, in *Thermodynamics*, edited by M. Tadashi (InTech, 2011), chap. 13, pp. 275–292.

[11] L. Onsager, Phys. Rev. **37**, 405 (1931).

[12] L. Onsager, Phys. Rev. **38**, 2265 (1931).

[13] H. B. Callen, Phys. Rev. **73**, 1349 (1948).

[14] T.-Y. Wu, Int. J. Theor. Phys. **2**, 325 (1969).

[15] T. J. Scheidemantel, C. Ambrosch-Draxl, T. Thonhauser, J. V. Badding, and J. O. Sofo, Phys. Rev. B **68**, 125210 (2003).

[16] J. Sofo and G. Mahan, Physical Review B **58**, 15620 (1998).

[17] V. R. Saunders, C. Freyria-Fava, R. Dovesi, L. Salasco, and C. Roetti, Mol. Phys. **77**, 629

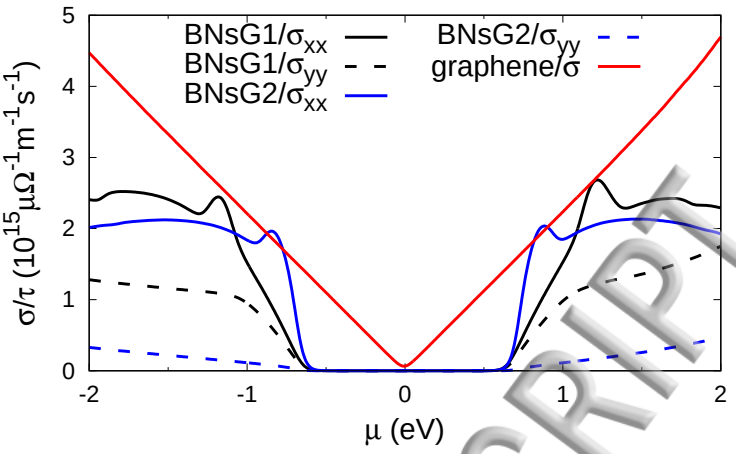

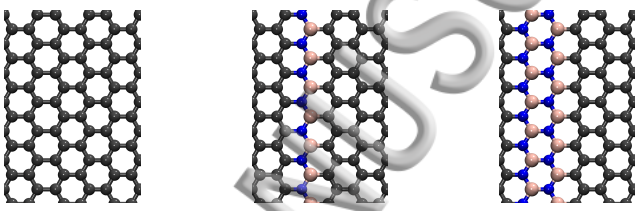

(b) Graphene (c) BNsG1 (d) BNsG2

Figure 4: In panel (a),the conductivity is reported as computed for pure graphene – depicted in panel (b) – and for two Boron-Nitride substituted Graphene (BNsG) – as seen in panels (c) and (d). The conductivities in the direction parallel (σ_{xx}) and perpendicular (σ_{yy}) to the ribbons are reported for the latter.

(1992).

[18] L. Maschio, B. Kirtman, M. Rérat, R. Orlando, and R. Dovesi, J. Chem. Phys. **139**, 164102 (2013).

[19] L. Maschio, B. Kirtman, R. Orlando, and M. Rérat, J. Chem. Phys. **137**, 204113 (pages 11) (2012).

[20] B. Champagne and J.-M. André, Int. J. Quant. Chem. **42**, 1009 (1992).

[21] P. Otto, F. L. Gu, and J. Ladik, J. Chem. Phys. **110**, 2717 (1999).

[22] C. E. Dykstra and P. C. Jasien, Chem. Phys. Lett. **109**, 388 (1984).

[23] M. Ferrero, M. Rérat, R. Orlando, and R. Dovesi, J. Comput. Chem. **29**, 1450 (2008).

[24] A. Ferretti, G. Mallia, L. Martin-Samos, G. Bussi, A. Ruini, B. Montanari, and N. M. Harrison, Phys. Rev. B **85**, 235105 (2012).

[25] R. D. *et al.*, in preparation (2017).

[26] L. Maschio, in preparation (2017).

[27] P. A. M. Dirac, in *Mathematical Proceedings of the Cambridge Philosophical Society* (Cambridge Univ Press, 1930), vol. 26, pp. 376–385.

[28] J. P. Perdew and A. Zunger, Phys. Rev. B **23**, 5048 (1981).

[29] J. P. Perdew, J. A. Chevary, S. H. Vosko, K. A. Jackson, M. R. Pederson, D. J. Singh, and C. Fiolhais, Phys. Rev. B **46**, 6671 (1992).

[30] J. P. Perdew, K. Burke, and M. Ernzerhof, Phys. Rev. Lett. **77**, 3865 (1996).

[31] Z. Wu and R. E. Cohen, Phys. Rev. B **73**, 235116 (2006).

[32] Z. Wu and R. E. Cohen, Phys. Rev. B **78**, 197102 (2008).

[33] A. D. Becke, J. Chem. Phys. **98**, 5648 (1993).

[34] C. Lee, W. Yang, and R. G. Parr, Phys. Rev. B **37**, 785 (1988).

[35] C. Adamo and V. Barone, J. Chem. Phys. **110**, 6158 (1999).

[36] T. Bredow and A. R. Gerson, Phys. Rev. B **61**, 5194 (2000).

[37] Y. Zhao and D. G. Truhlar, Theor. Chem. Acc. **120**, 215 (2008).

[38] A. V. Krukau, O. A. Vydrov, A. F. Izmaylov, and G. E. Scuseria, J. Chem. Phys. **125**, 224106 (2006).

[39] E. Weintraub, T. M. Henderson, and G. E. Scuseria, J. Chem. Theory Comput. **5**, 754 (2009).

[40] C. Kittel, *Introduction to Solid State Physics* (John Wiley & Sons, Inc., Hoboken, NJ, 2005), 8th ed.

[41] O. Madelung, *Semiconductors: Data Handbook* (Springer, New York, 2004), 3rd ed.

[42] J. M. Crowley, J. Tahir-Kheli, and W. A. Goddard, The Journal of Physical Chemistry Letters **7**, 1198 (2016).

[43] J. M. Crowley, J. Tahir-Kheli, and W. A. Goddard, The Journal of Physical Chemistry Letters **6**, 3792 (2015).

[44] B. Goltsman, B. Kudinov, and I. Smirnov, Tech. Rep., DTIC Document (1973).

[45] K. Koga, K. Akai, K. Oshiro, and M. Matsuura, Phys. Rev. B **71**, 155119 (2005).

[46] I. Aguilera, C. Friedrich, and S. Blügel, Phys. Rev. B **88**, 165136 (2013).

[47] L. Maschio, M. Lorenz, D. Pullini, M. Sgroi, and B. Civalleri, Phys. Chem. Chem. Phys. **18**, 20270 (2016).

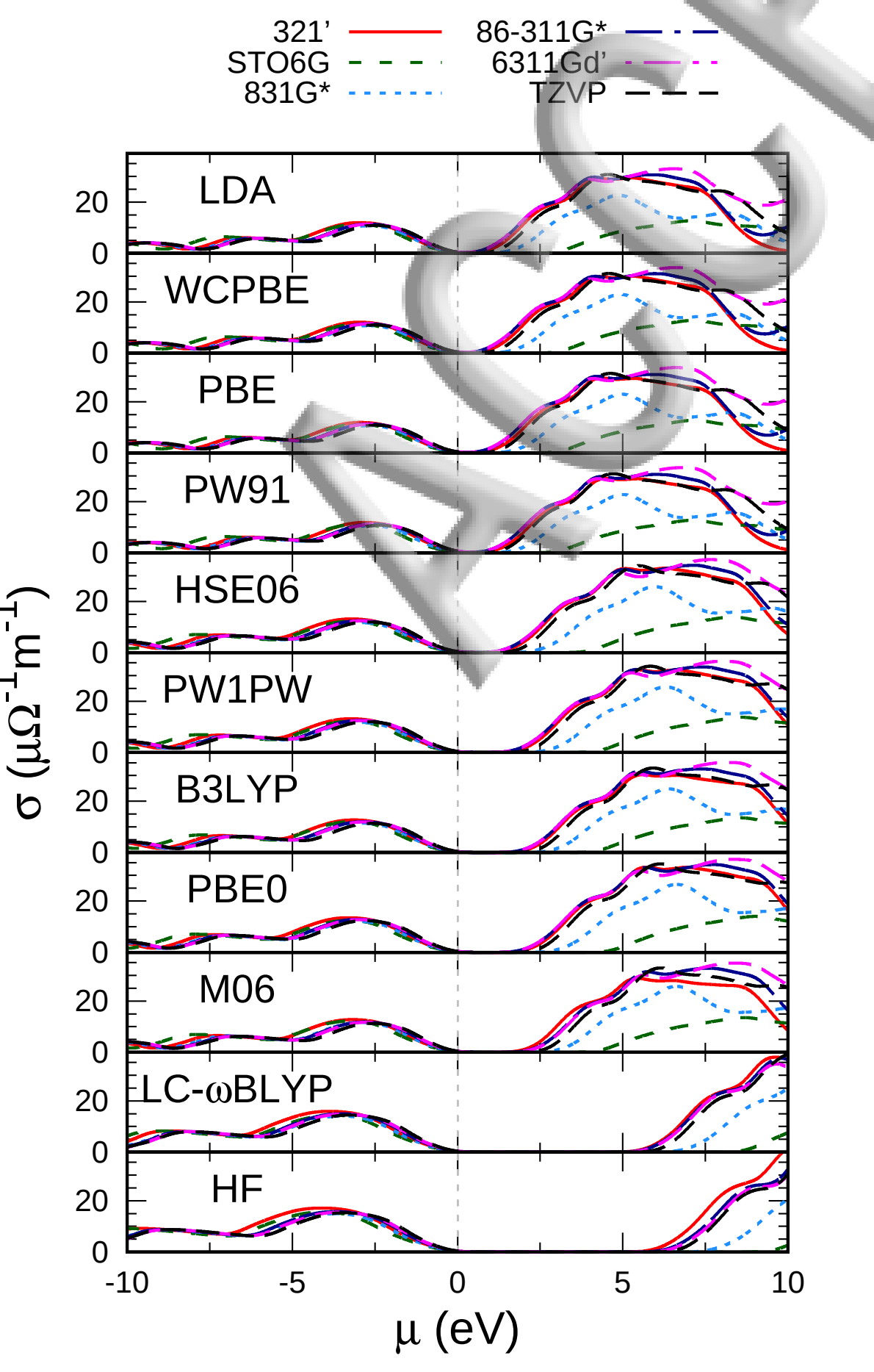
321'
STO6G
831G*
86-311G*
6311Gd'
TZVP
LDA
WCPBE
PBE
PW91
HSE06
PW1PW
B3LYP
PBE0
M06
LC-ωBLYP
HF
20
0
-10
-5
0
5
10
σ (μΩ-1m-1)
μ (eV)

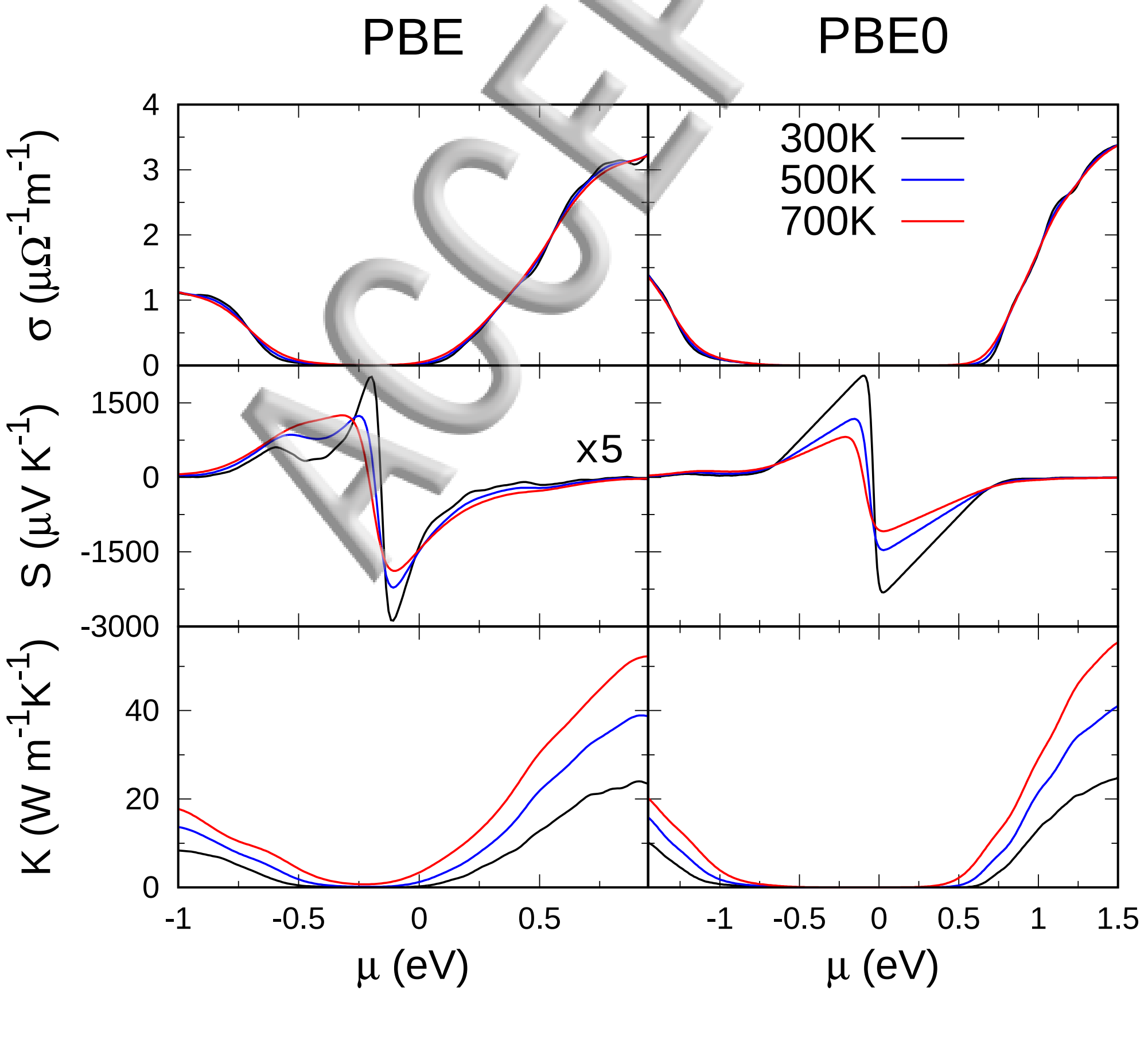
PBE
PBE0
300K
500K
700K
x5
σ (μΩ-1m-1)
S (μV K-1)
K (W m-1K-1)
μ (eV)
μ (eV)

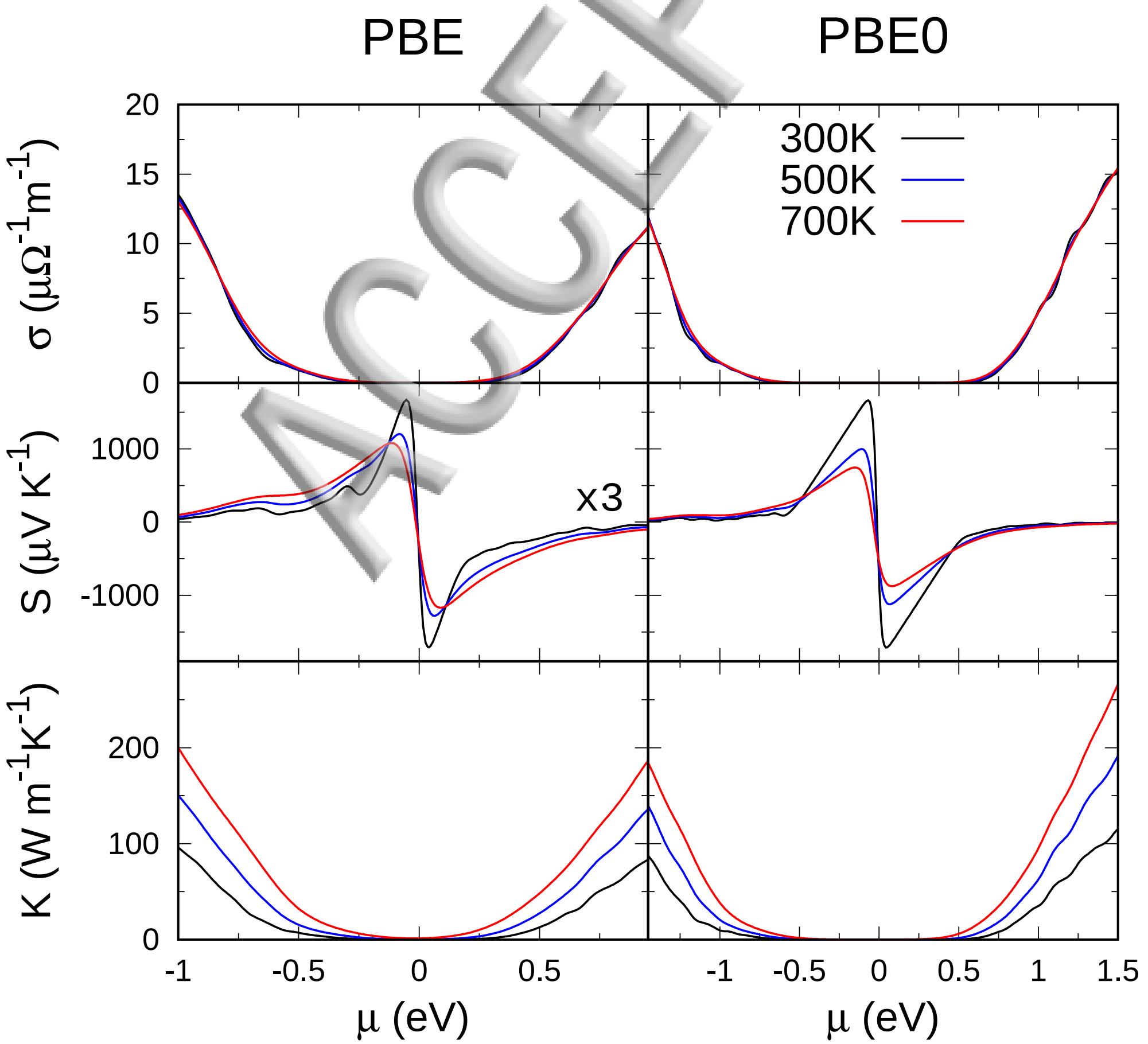
PBE
PBE0
300K
500K
700K
x3
σ (μΩ-1m-1)
S (μV K-1)
K (W m-1K-1)
μ (eV)
μ (eV)
20
15
10
5
0
1000
0
-1000
200
100
0
-1
-0.5
0
0.5
1
1.5

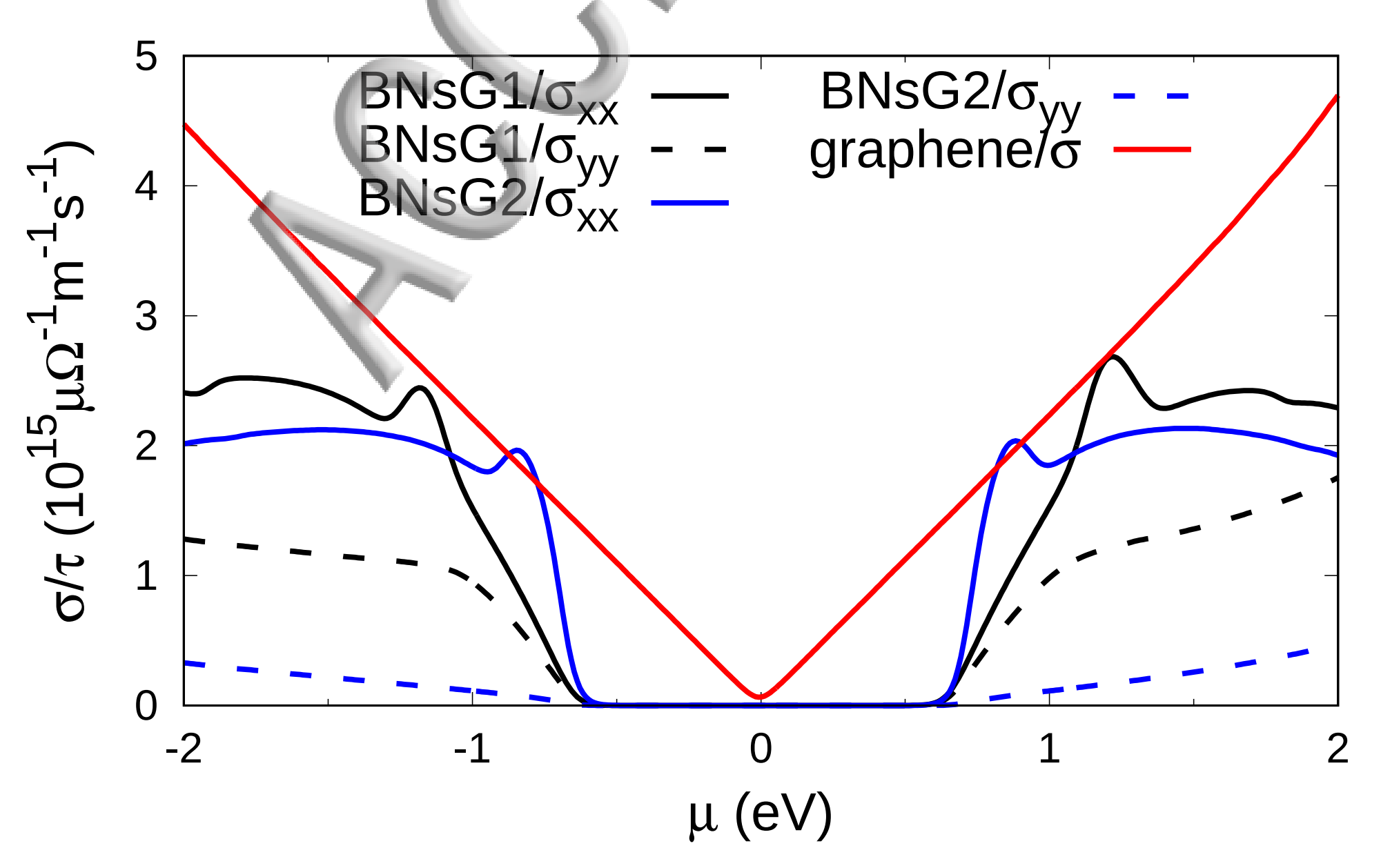
BNsG1/σxx
BNsG1/σyy
BNsG2/σxx
BNsG2/σyy
graphene/σ
σ/τ (10^15 μΩ^-1 m^-1 s^-1)
μ (eV)
5
4
3
2
1
0
-2
-1
0
1
2